Graphitic Carbon Nitride Sputtered with Silver Nanoparticles for Efficient Photocatalytic Degradation of Rhodamine B Dye

Lifeng Cui[†,*], Tingting Pu[†], Xueyou Fang[†], Jialing Song, Shasha Li, Junjie Wang,
Chaochuang Yin, Huancong Shi, Shifei Kang

Department of Environmental Science and Technology, University of Shanghai for Science and Technology, Shanghai 200093, China
[†] These authors contributed equally to this work and should be considered co-first authors.
[*]E-mail: lifeng.cui@gmail.com

Graphitic carbon nitride (g-C_3N_4) powder was synthesized using a thermal polymerization method. Silver nanoparticles were uniformly deposited on thin sheets of g-C_3N_4 using a simple sputtering method. Pure g-C_3N_4 and Ag/g-C_3N_4 were tested for photocatalytic degradation performance of Rhodamine B dye under visible light. The degradation tests show that photocatalytic activity of heterostructured Ag/g-C_3N_4 was greatly enhanced compared with that of pure g-C_3N_4 even with as little as 0.08 wt% added silver. The percentage of silver used is significantly lower than that used in previous studies of Ag/g-C_3N_4 composite catalysts. The Ag/g-C_3N_4 catalyst also shows excellent stability over multiple reaction cycles.

1. INTRODUCTION

Water pollution has become a growing threat to environment and human health. Organic dyes and inorganic heavy metal ions are major causes for water pollution because they are difficult to degrade by natural means [1]. Semiconductor photocatalysis is known as a promising route to treat pollutants in water and also an environmentally friendly approach [2-5]. However most semiconductor photocatalysts can only absorb ultraviolet light (4% of solar energy), which seriously restrict their practical applications [6,7]. Visible light energy, which accounts for about 48% of the incoming solar energy, is more abundant than ultraviolet light energy. Therefore, the development of visible light

responsed photocatalysts for efficient utilization of the solar energy has become a research hotspot in recent years [8,9].

G-C_3N_4, as a n-type semiconductor (Eg = 2.7 eV) which contains no metallic elements, has attracted enormous research interests because of its extensive applications in lithium ion battery [10], dye-sensitized solar cells [11], hydrogen evolution [12] and pollutant degradation [13]. In order to overcome its intrinsic shortcoming of low efficiency and to enhance its catalytic performances, different types of g-C_3N_4-based heterostructures with various band edge positions have been investigated by many researchers. To date, a few reports in the literature have studied Ag/g-C_3N_4 nanocomposites for photocatalytic degradation. Zhang prepared Ag modified g-C_3N_4 composite photocatalysts by photodeposition method. When the amount of Ag was as high as 54%, the composite catalyst Ag/g-C_3N_4 showed the best activity for diclofenac degradation [14]. Bu successfully deposited Ag nanoparticles (NPs) onto mesoporous g-C_3N_4 using photo-assisted reduction method. They found that 3 wt% Ag in the Ag/g-C_3N_4 composite demonstrated the best photocatalytic RhB degradation efficiency attributed this improvement to the enhanced separation of photo-generated electrons and holes [15].

In this study, we deposited silver nanoparticles on g-C_3N_4 nanosheets using a simple sputtering method. The TEM studies showed that the silver nanoparticles were dispersed evenly, and the size was uniform. It is worth mentioning that the amount of silver used in this paper is as low as 0.08 wt% and the heterostructured catalyst shows excellent performance in degradation test of RhB under visible light.

2. EXPERIMENTAL SECTION

2.1. Reagents

Ultrapure deionized water (>18 MΩ cm), produced with a Millipore system, was used for the preparation of all experimental solutions. All chemicals were of reagent grade and were used without further purification or treatment.

2.2. Preparation of g-C_3N_4 and Ag/g-C_3N_4 sample

The g-C_3N_4 powder was prepared using a thermal polymerization method. Briefly, 5g of urea was added into a crucible with a cover, and heated to 794 K in a muffle furnace at a heating rate of 15 K per minute from room temperature. The temperature was maintained at 794 K for 3 h. After naturally cooling down to room temperature, the residual g-C_3N_4 product was collected and grounded into yellow powder.

Ag/g-C_3N_4 heterostructured photocatalyst was prepared by a simple sputtering method. As shown in Fig. 1, 0.5 g of as-prepared bulk g-C_3N_4 was grounded into powder and then added into 50 mL of methanol. After 0.5 h of ultrasonic treatment, methanol was removed by continuous insufflation of N_2. A small amount (0.1 g) of ultrasonic treated g-C_3N_4 was very thinly tiled on the evaporating

dish, and then the evaporating dish was placed in a sputtering apparatus. The sputtering current was set to a relatively small value (2 mA) and then the apparatus was turned on to start the sputtering. After a certain time of sputtering, the instrument was turned off and the sample was collected. The $Ag/g\text{-}C_3N_4$ samples, which were sputtered with 5, 10, 15, 20 and 300 s, were labeled as AgCN5, AgCN10, AgCN15, AgCN20 and AgCN300, respectively.

The percentage of silver in the AgCN10 catalyst was estimated to be 0.08 wt% by comparing the weight of the sample on the evaporating dish before and after sputtering.
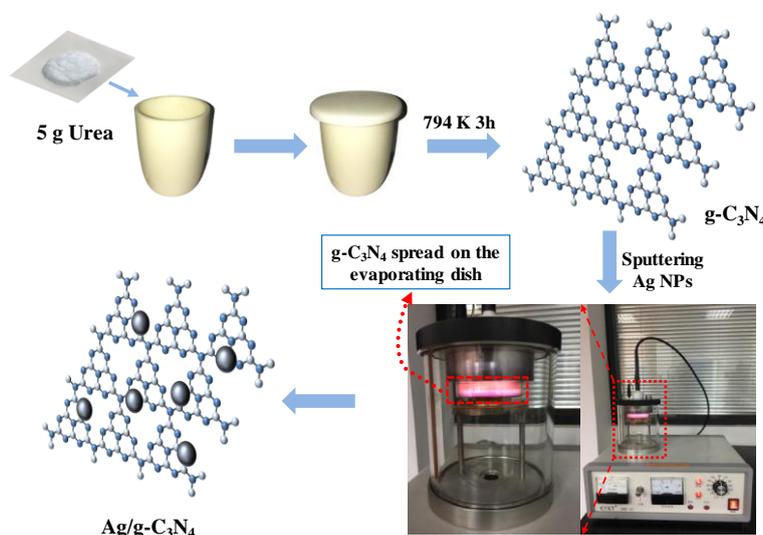
Figure 1. Preparation flow chart of $Ag/g\text{-}C_3N_4$

2.3. Characterization methods

Crystal structures of the products were identified by X-ray powder diffractometer (XRD) with Cu Kα irradiation (λ = 1.54 Å) at 40 KV, 30mA, and a scan rate of 2° min^{-1}. The morphologies and microstructures of the photocatalyst samples were characterized by transmission electron microscopy (TEM, JEOL, JEM-2010). The X-ray photoelectron spectroscopy (XPS) measurements were done on a Thermo Scientific ESCALAB 250 instrument meter with Al Kα source. The binding energies (Eb) were calibrated internally by the carbon deposit C1 s binding energy at 284.6 eV. The UV-vis absorption spectra of the samples were collected with a UV-vis spectrophotometer (Shimadzu, Japan, UV-2401) in the range of 200-800 nm. $BaSO_4$ was the reflectance sample.

2.4. Evaluation of photocatalytic activity

The photocatalytic activities of the as-prepared $g\text{-}C_3N_4$ nanosheets and $Ag/g\text{-}C_3N_4$ were evaluated by the degradation of Rhodamine B (RhB) under visible light irradiation. The light source was a 300 W Xenon lamp equipped with a cut-off filter ($\lambda \geq$ 420 nm), the illumination intensity was 100 mW cm^{-2}. In a typical run, 30 mg of the photocatalyst powder was suspended in 50 mL of 20 mg L^{-1} RhB aqueous solution in a quartz tube reactor. In the experiment process, the reaction system was

cooled by water circulation, and the temperature was maintained at 293 K. The aqueous samples were collected at regular intervals and filtrated through 0.45 μm membranes. The photodegradation over RhB was also performed without any photocatalyst under the same condition.

2.5. Photoelectrochemical measurements

Transient photocurrent responses and the electrochemical impedance spectroscopy (EIS) measurements were performed with a CHI 660E potentiostat in a standard three-electrode cell system. An Ag/AgCl electrode was used as the reference electrode and a Pt plate was used as the counter electrode. The working electrode was prepared by taking active material (Ag/g-C_3N_4 composites), conductive additive (carbon black), and binder (PVDF) at the weight ratio (8:1:1) and mixed together into a N-methyl pyrrolidone solvent to obtain the slurry. The resulting slurry was coated onto the ITO plate (an active area of 1 cm^2) and dry at 333 K in an oven for overnight. A 0.5 M Na_2SO_4 solution was used as the electrolyte. A 300 W Xe lamp equipped with a UV cut-off filter ($\lambda \geq 420$ nm) served as the visible light source. The photoresponsive signals of the samples were measured under chopped light at 0.0 V.

3. RESULTS AND DISCUSSION
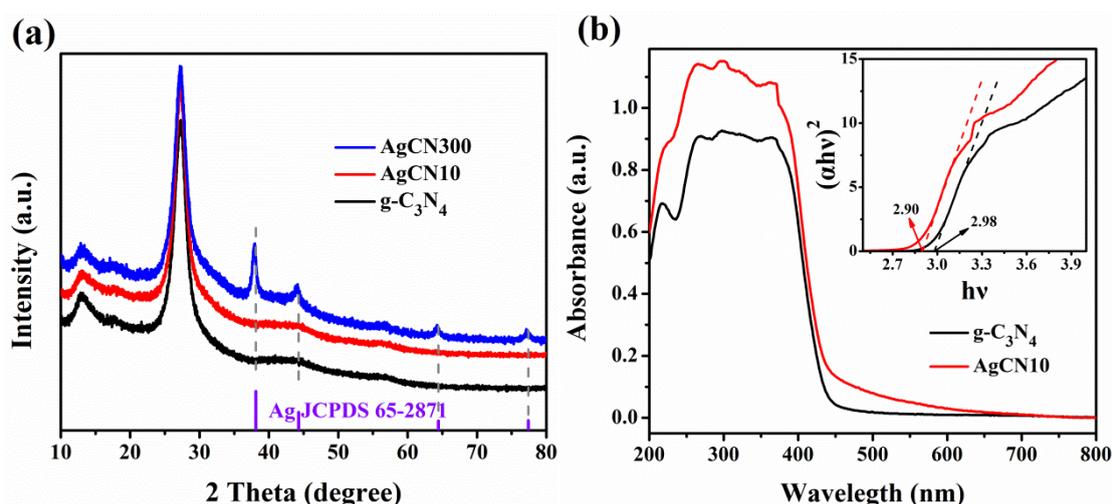
Figure 2. (a) Power XRD patterns, (b) UV-visible absorbance spectra and plots of $(\alpha h\nu)^2$ versus photon energy (b inset) of g-C_3N_4 and AgCN10.

To investigate the crystal structure of pure g-C_3N_4 nanosheets and AgCN10 powder, XRD was carried out. From Fig. 2a, the XRD pattern of pure g-C_3N_4 is indexed as JCPDS No. (87-1526) [16]. Compared with the pure g-C_3N_4, after being sputtered for 10 seconds, there is no obvious peak of Ag appeared, ascribing to trace amounts of silver. After being sputtered for a long period of 300 seconds, there are four distinct diffraction peaks of pure Ag appeared in the spectra. The peaks located at 38.1°,

$44.2°$, $64.4°$, $77.4°$ can be indexed to the diffraction of (111), (200), (220), and (311) lattice planes of crystalline silver (JCPDS No. 65-2871) [17]. These results confirmed the existence of Ag NPs on the g-C_3N_4 nanosheets, and they are consistent well with the HRTEM observations.

The optical properties of the g-C_3N_4 nanosheets and AgCN10 were carried out by the UV-vis absorption spectra (Fig. 2b). Compared with the pure g-C_3N_4, AgCN10 showed increased absorption of visible light after the sputtering of Ag NPs. As shown in Fig. 2b inset, the optical bandgaps of g-C_3N_4 and AgCN10 were calculated as 2.98 eV and 2.90 eV. The band gap of AgCN10 reduces after the sputtering of Ag NPs that promoted the utilization of low-energy photons in degradation of RhB.

The morphology and microstructure of the AgCN10 photocatalyst were investigated by TEM. Fig. 3 shows the TEM micrograph of AgCN10. The uniform dispersion of numerous dark grey colored spots with the diameter of ~10 nm indicate a high deposition of Ag NPs on the surface of g-C_3N_4. The inset figure in Fig. 3 shows the lattice image of the Ag NPs, the characteristic values of lattice constant are 0.24 and 0.20 nm corresponding to the typical (111) and (200) crystal phase of Ag, respectively [18,19].
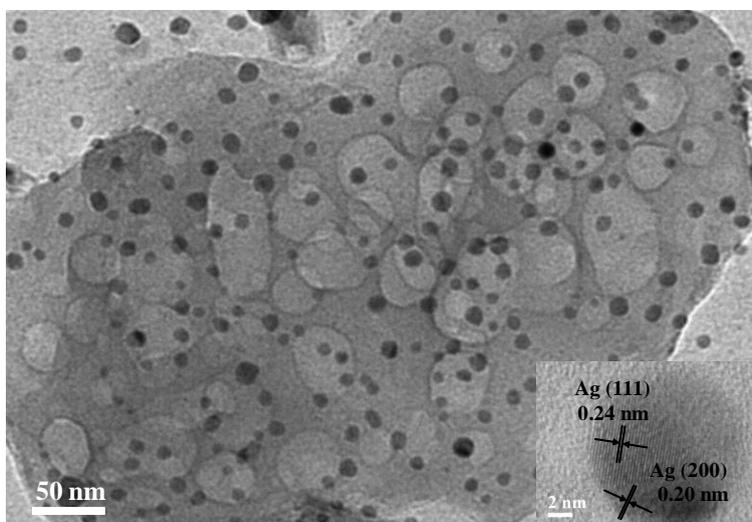
Figure 3. TEM of AgCN10 (inset: high-magnification TEM image of a Ag NP).

XPS spectra of AgCN10 were obtained for the analysis of the structure and surface of the composite catalyst (Fig. 4). The survey scan spectrum of AgCN10 showed peaks for C, N and Ag (Fig. 4a). The C 1s (Fig. 4b) spectra of AgCN10 could be fitted to four peaks at 284.7, 285.1, 288.3, and 288.6 eV, which could be attributed to the sp^2 C-C bonds, C-NH_2 species, N=C-N coordination and the N-C-O groups, respectively [20,21]. In the N 1s spectrum (Fig. 4c), four peaks at 398.2, 399.1, 400.4 and 401.8 eV can be attributed to pyridinc-like N, pyrrolic-like N, graphitic-like N and N-H, respectively [22]. Fig. 4d showed the characteristic Ag 3d peaks at 368.2 and 374.2 eV with 6.0 eV splitting, which corresponds to the metallic Ag^0 species [23].
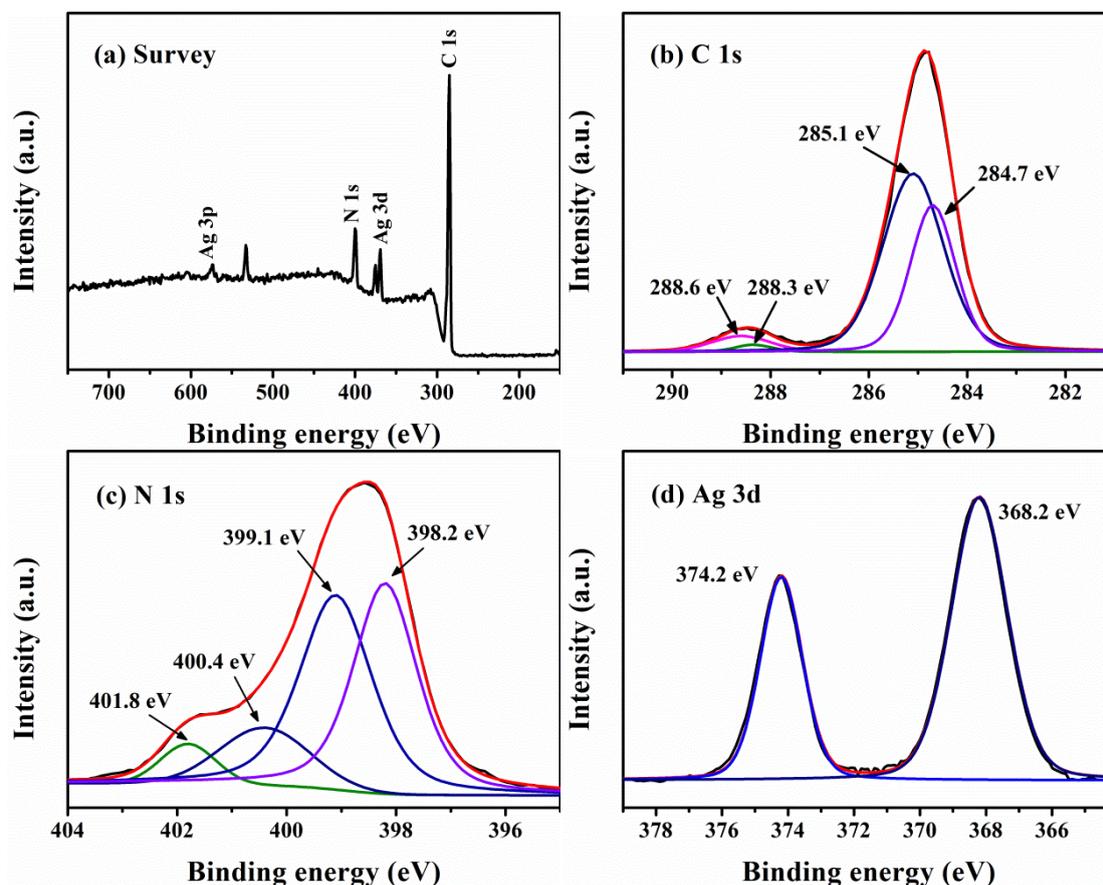
Figure 4. XPS spectra of AgCN10: (a) survey XPS spectrum; (b) C 1s; (c) N 1s; (d) Ag 3d.

In order to investigate the excitation and transfer of photo-induced charge carriers among photocatalysts, the transient photocurrent responses and EIS measurements were performed. This photocurrent increases when exposed to a light source, and it indicates that the photo-generated electrons migrate in the bulk materials to produce photocurrent (Fig. 5a) [24]. The photogenerated current densities of pure g-C_3N_4 and AgCN10 under visible light were 0.81 and 1.37 $\mu A\ cm^{-2}$, respectively. The higher photocurrent intensity led to lower recombination speed of photo-induced electrons and holes, so we could find out the AgCN10 photocatalyst owned better separation rate of photo-generated electron-hole pairs compared with pure g-C_3N_4 photocatalyst. Fig. 5b shows the EIS date of AgCN10 and g-C_3N_4 nanosheets. The diameter of the Nyquist semicircle of AgCN10 is smaller than that of pure g-C_3N_4 [25], and implies that the AgCN10 has a smaller charge transfer resistance, which reflects the effective separation of electrons and holes.

RhB was chosen to evaluate the photocatalytic performances of Ag/g-C_3N_4 photocatalyst at room temperature. Before visible light irradiation, the RhB solutions containing photocatalyst were stirred in the darkness for 0.5 h to achieve adsorption equilibration. Fig.6a shows the RhB degradation curves with catalyst, in which C_0 is the RhB concentration after adsorption equilibration, and C represents the instantaneous concentration of RhB at time t. The concentration of remnant RhB decreased with the time taken for photocatalysis, and the RhB degradation efficiencies indicated that RhB was decreased faster by Ag/g-C_3N_4 than by the g-C_3N_4 nanosheets.
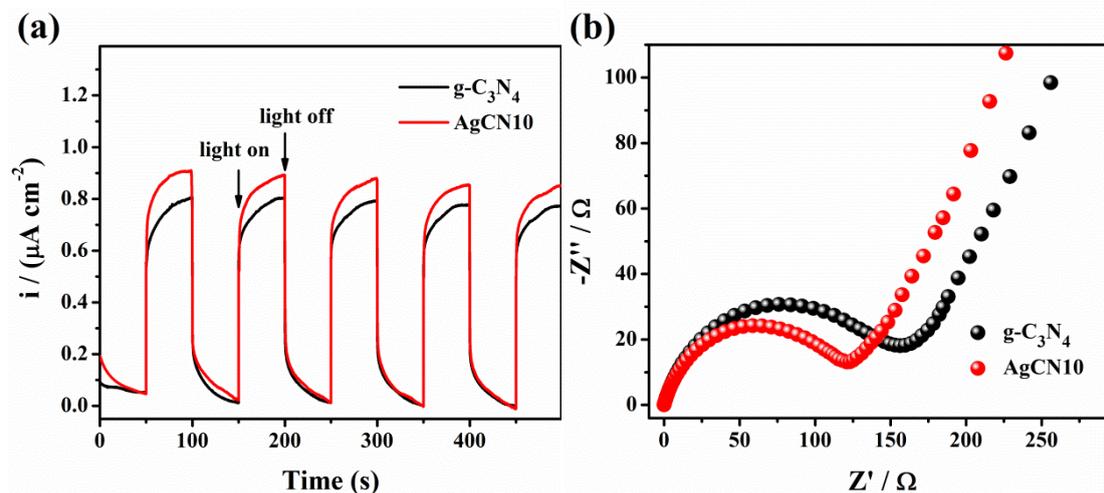
Figure 5. Photocurrent responses and EIS spectra of pure g-C$_3$N$_4$ and AgCN10 under visible light irradiation.

It is shown from the photocatalytic results that the AgCN10 photocatalyst was more efficient for the degradation of RhB than Ag/g-C$_3$N$_4$ composite with other sputtering time. Furthermore, the result in Fig. 6b shows no strong reduction in photocatalytic activity after four consecutive cycling tests. The results indicated that the photocatalyst AgCN10 exhibited good stability for the photodegradation of RhB under visible light.
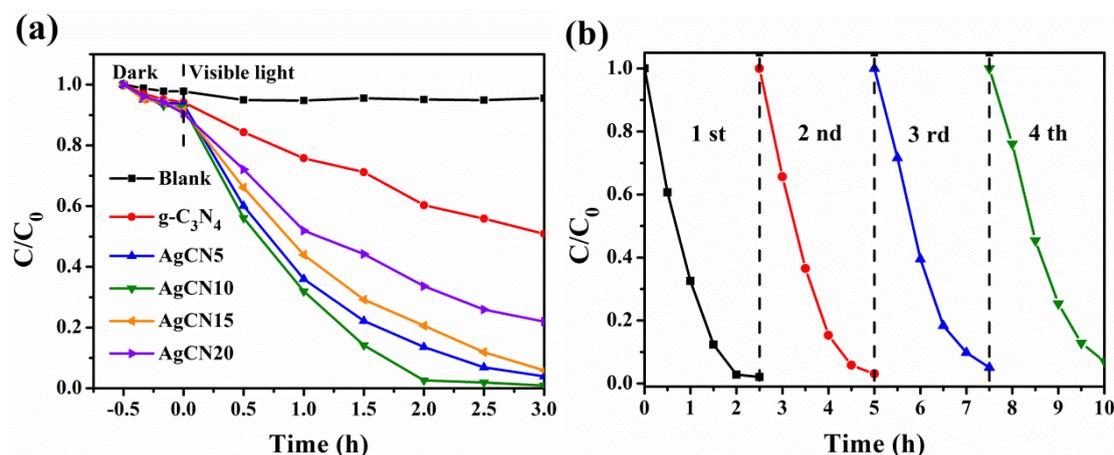
Figure 6. (a) Photocatalytic degradation curves of g-C$_3$N$_4$ and Ag/g-C$_3$N$_4$ samples and (b) Recyclability of AgCN10 for RhB dye degradation under visible light irradiation ($\lambda \geq 420$ nm)

The recent literature on the degradation of RhB with Ag/g-C$_3$N$_4$ composite was investigated, as shown in Table 1. Comparing with pure g-C$_3$N$_4$, modifying g-C$_3$N$_4$ with Ag has greatly improved the photocatalytic degradation efficiency, which demonstrates that Ag/g-C$_3$N$_4$ composite is very good photodegradation catalyst. It is worth mention that a simple method is used in our work with less amount of Ag can achieve a good degradation effect.

Table 1. Comparison of RhB degradation using Ag/g-C$_3$N$_4$ composite

Synthesis method of catalyst	Optimum concentration of Ag	C$_0$ of RhB (mg L^{-1})	Time required when C/C$_0$ = 0.8	Ref
Ag/C$_3$N$_4$ photocatalysts were synthesized using NaBH4 and the squeezed out liquid of watermelon rind.	0.48%	20	3 h	[26]
A rapid microwave-assisted synthesis of Ag/g-C$_3$N$_4$ photocatalysts in ethylene glycol.	2%	10	80 min	[27]
Melamine, AgNO$_3$ and NH$_4$Cl were heated to 550 °C for 4 h.	2%	10	34 min	[28]
Ag/D-C$_3$N$_4$ was synthesized by direct calcining DCDA, AgNO$_3$ and melamine precursors.	--	10	54 min	[29]
Irradiated for 3 h using a 300 W Xenon lamp under vigorous stirring.	3 wt%	10	12 min	[15]
Irradiated by 800 W Xenon lamp with continuous stirring for 0.5 h.	8 wt%	10	20 min	[30]

Based on the above results, we propose a tentative reaction mechanism for photocatalytic degradation of RhB over the Ag/g-C$_3$N$_4$ composites (Fig. 7). The g-C$_3$N$_4$ nanosheets can be excited to generate electrons and holes under visible light irradiation. In the Ag/g-C$_3$N$_4$ composites, a Schotky barrier junction can be produced by Ag NPs and g-C$_3$N$_4$ nanosheets, which can effectively enhance both recombination time and separation of photo-induced electrons and holes. Photo-induced charge carriers can react with OH$^-$ and O$_2$ to form •OH and •O$_2$$^-$, and the active species are promoted due to surface plasmon resonance (SPR) effect of Ag. The possible photocatalytic reactions and degradation of RhB are listed in the following:

$$\text{Ag/g-C}_3\text{N}_4 + hv \rightarrow \text{Ag/g-C}_3\text{N}_4 \ (e^- + h^+) \tag{1}$$

$$\text{OH}^- + h^+ \rightarrow •\text{OH} \tag{2}$$

$$e^- + \text{O}_2 \rightarrow •\text{O}_2^- \tag{3}$$

$$•\text{O}_2^-, •\text{OH} + \text{RhB} \rightarrow \text{CO}_2 + \text{H}_2\text{O} \tag{4}$$
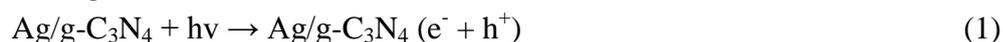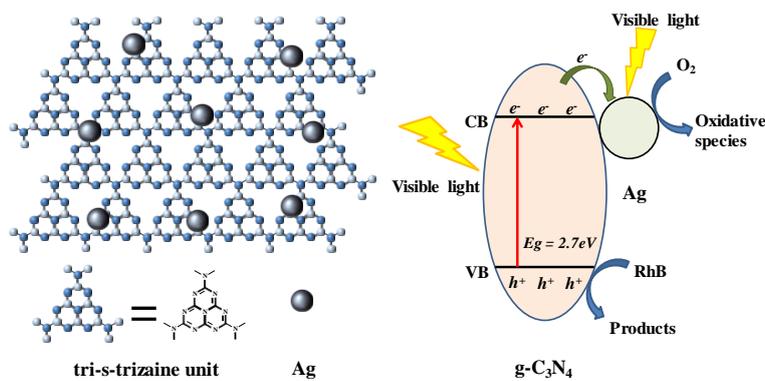
Figure 7. A diagram of the Ag/g-C$_3$N$_4$ composite (left) and Schematic diagram illustrating the photocatalytic degradation of RhB under visible light irradiation (right).

4. CONCLUSION

A novel visible-light-driven heterostructured Ag/g-C$_3$N$_4$ photocatalyst was synthesized using a simple sputtering method. Although the amount of silver used in this work is very small (0.08 wt%) compared with previous studies of Ag/g-C$_3$N$_4$ composite catalysts, a great photodegradation catalytic performance was achieved. The TEM spectra shows that numerous Ag NPs about 10 nm in diameter were uniformly deposited on the surface of g-C$_3$N$_4$ nanosheets. The photodegradation performance of Ag/g-C$_3$N$_4$ photocatalyst was significantly improved compared with that of pure g-C$_3$N$_4$. The mechanism of enhanced photocatalytic performance toward RhB degradation was experimentally investigated via UV-vis DRS, photocurrent responses and EIS spectra. The enhanced photocatalytic performance was attributed to combining effects of good interfacial junction between Ag NPs and g-C$_3$N$_4$ nanosheets, which led to increased optical absorption in the visible region, quick separation and transportation of photo-induced electrons and holes, and long lifetime of charge carriers as well.

References

1. I.Ali, *Chem. Rev.*, 112 (2012) 5073.
2. Y.H. Sang, Z.H. Zhao, M.W. Zhao, P. Hao, Y.H. Leng and H. Liu, *Adv. Mater.*, 27 (2015) 363.
3. D.P. Zhang, S.H. Cui and J. Yang, *J. Alloy. Compd.*, 708 (2017) 1141.
4. Y.W. Gao, Y. Wang and H. Zhang, *Appl. Catal.* B., 178 (2015) 29.
5. H.J. Huang, J. Zhang, L. Jiang and Z.G. Zang, *J. Alloy. Compd.*, 718 (2017) 112.
6. D.J. Yang, C.C. Chen, Z.F. Zheng, H.W. Liu, E. R. Waclawik, Z.M. Yan, Y. Huang, H.J. Zhang, J.C. Zhao and H.Y. Zhu, *Energy Environ. Sci.*, 4 (2011) 2279.
7. Q.Z. Wang, G.X. Yun, Y. Bai, N. An, J.H. Lian, H.H. Huang and B.T. Su, *Appl. Surf. Sci.*, 313 (2014) 537.

8. C. Yang, S.C. Wu, J.H. Cheng and Y.C. Chen, *J. Alloy. Compd*., 687 (2016) 804.
9. Z.W. Tong, Y. Dong, L. Zhen, Y.H. Nan, F. Ding, Y.C. Shen and Z.Y. Jiang, *Acs Nano*., 11 (2016) 1103.
10. M.J. Shi, T.H. Wu, X.F. Song, J. Liu, L.P. Zhao, P. Zhang and L. Gao, *J. Mater. Chem. A*., 4 (2016) 10666.
11. J. Xu, G.X. Wang, J.J. Fan, B.S. Liu, S.W. Cao and J.G. Yu, *J. Power Sources*., 274 (2015) 77.
12. X.Y. Fang, J.L. Song, H.C. Shi, S.F. Kang, Y. Li, G.W. Sun and L.F. Cui, *Int. J. Hydrogen Energ*., 42 (2017) 5741.
13. J.Z. Wang, S.Y. Dong, C.F. Yu, X. Han, J.Y. Guo and J.H. Sun, *Catal. Commun*., 92 (2017) 100.
14. W. Zhang, L. Zhou and H.P. Deng, *J. Mol. Catal. A: Chem*., 423 (2016) 270.
15. Y.Y. Bu, Z.Y. Chen and W.B. Li, *Appl. Catal. B*., 144 (2014) 622.
16. L. Zhou, W. Zhang, L. Chen, H.P. Deng and J.L. Wan, *Catal. Commun*., 100 (2017) 191.
17. X. He, R.H. He, A. L. Liu, X.Y. Chen, Z.L. Zhao, S. Feng, N. Chen and M. Zhang, *J. Mater. Chem. C*., 2 (2014) 9737.
18. H.M. Dai, N. Cao, L. Yang, J. Su, W. Luo and G.Z. Cheng, *J. Mater. Chem. A.*, 2 (2014) 11060.
19. S. Sareen, V. Mutreja, S. Singh and B. Pal, *RSC Adv*., 5 (2015) 184.
20. J.H. Li, B. Shen, Z.H. Hong, B.Z. Lin, B.F. Gao and Y.L. Chen, *Chem. Commun*., 48 (2012) 12017.
21. B.H. Long, J.L. Lin and X.C. Wang, *J. Mater. Chem. A*., 2 (2014) 2942.
22. M. Yan, Y.Q. hua, F.F. Zhu, L. Sun, W. Gu and W.D. Shi, *Appl. Catal. B*., 206 (2017) 531.
23. L. Ge, C.C. Han, J. Liu and Y.F. Li, *Appl. Catal. A*., 409 (2011) 215.
24. L. Li, Y.H. Qi, J.R. Lu, S.L. Lin, W. J.An, Y.H. Liang and W.Q. Cui, *Appl. Catal. B*., 183 (2015) 133.
25. D.S. Wang, Z.X. Xu, Q.Z. Luo, X.Y. Li, J. An, R. Yin and C. Bao, *J. Mater. Sci*., 51 (2016) 893.
26. K. Tian, W.J. Liu and H. Jiang, *Acs. Sustain. Chem. Eng* ., 3 (2015) 269.
27. T. Sun, H.Y. Jiang, C.C. Ma, F. Mao and B. Xue, *Catal. Commun*., 79 (2016) 45.
28. J. Jin, Q. Liang, C.Y. Ding, Z.Y. Li and S. Xu, *J. Alloy. Compd*., 691 (2017) 763.
29. C.Y. Min, C. Shen, R. Li, Y. Li, J.L. Qin and X.F. Yang, *Ceram. Int*., 42 (2016) 5575.
30. Z.J. Li, J.H. Wang, K.X. Zhu, F.L. Ma and A. Meng, *Mater. Lett*., 145 (2015) 167.